ISSN 1392-1207. MECHANIKA. Vol. 31, No. 3, 2025: 211–219

Effect of Surface Thermoelastic Deformation on the Performance of the Hydrodynamic Big-Size Step Bearing

Xiang YE*, Yongbin ZHANG**
**College of Mechanical Engineering, Changzhou University, Changzhou, Jiangsu Province, China*
***College of Mechanical Engineering, Changzhou University, Changzhou, Jiangsu Province, China,*
E-mails: yongbinzhang@cczu.edu.cn, engmech1@sina.com (Corresponding Author)
https://doi.org/10.5755/j02.mech.40713

1. Introduction

Hydrodynamic big-size thrust bearings have important applications in the large mechanical apparatus such as hydrogenerators and turbine machinery [1]. Their diameters can be several meters and they need to work with the loads even on the scale of 1×10^7 N and with the sliding speeds on the scales of 10m/s or 100m/s [2]. Classical hydrodynamic lubrication theory [3] predicts that there should still be sufficiently thick lubricating films in these bearings which can well separate the coupled bearing surfaces. But actually these bearings often suffered from film and pad failures with the surface seizure [4]. The effects of the fluid non-Newtonian shear thinning, the surface roughness and the fluid film viscous heating are unable to result in the film breakdown in the bearing [5-7]. It was popularly ascribed to the effect of the pad thermal distortion which is very pronounced for big-size thrust bearings [8-10].

There is some literature on theoretically studying the effect of the surface thermoelastic deformation in hydrodynamic lubricated thrust bearings by different methods [11-14]. These studies are based on continuum fluid lubrication and ignore the effect of the fluid molecule layers physically adsorbed to the bearing surfaces. However, when the lubricating film thickness is reduced to nearly vanishing, the effect of the physically adsorbed layer on the bearing surface should be very significant. Particularly for the thrust bearing with low clearances, the physically adsorbed molecule layers on the bearing surfaces may influence the shear stresses on the bearing surfaces, the frictional heating in the bearing and thus the thermal distortions of the bearing surfaces. The former studies lack in considering these important factors.

The present paper theoretically studies the performance of the hydrodynamic lubricated big-size step bearing by considering both the effects of the surface thermal distortion and the physically adsorbed molecule layer on the bearing surface. The surface thermal distortion is calculated from the formula given by Zhang [15]. The multiscale lubrication equation is applied to account for the effect of the physically adsorbed layer. The numerical solution procedure is developed. The film pressure, film thickness, carried load and friction coefficient of the bearing are calculated. The obtained results give us the new understanding on the performance of the big-size step bearing.

2. Hydrodynamic Big-Size Step Bearing with Surface Thermal Distortion

In hydrogenerators, hydro turbines and other large mechanical apparatus, hydrodynamic lubricated big-size thrust bearings are often used to support the axial load. Fig. 1 shows one of these types of bearings. Because of the big bearing width ($l_1 + l_2$) which can reach several meters, the thermal distortions of the bearing surfaces are very significant in the working condition of heavy loads and high sliding speeds due to the severe frictional heating; They can cause the great reduction of the lubricating film thickness and even the film vanishing [4, 8-10]. When the surface separation is as low as comparable to the thickness of the fluid molecule layers physically adsorbed to the bearing surfaces, which is normally on the 1nm scale or even bigger, the effect of the physically adsorbed layer on the bearing surface should be very significant [16]. Due to this reality, the present study considers the combined effects of the surface thermal distortion and the physically adsorbed layer to more truly reveal the bearing performance when the surface separation is over low.

In Fig. 1, $h_{tot,i}$ and $h_{tot,o}$ are the surface separations respectively on the entrance and the exit of the bearing, h_{bf} is the thickness of the adsorbed layer, Δh is the step size of the bearing, l_1 and l_2 are respectively the widths of the outlet and inlet zones of the bearing, and u is the sliding speed.

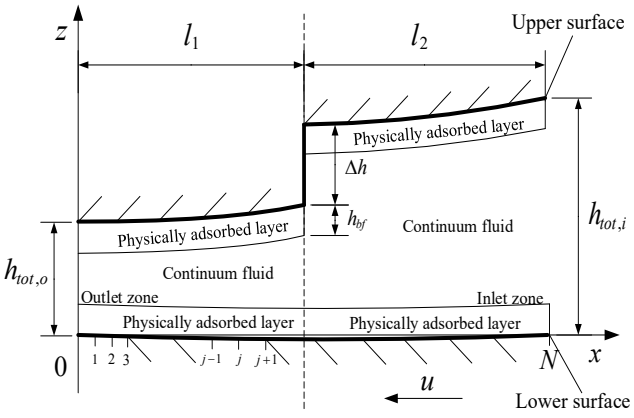

Fig. 1 The hydrodynamic big-size step bearing working in the condition of heavy loads and high sliding speeds involving the effects of the surface thermal distortion and the fluid molecule layers physically adsorbed to the bearing surfaces

3. Mathematical Analysis

3.1. Basic equations

The hydrodynamic lubrication in the present studied bearing is actually multiscale. Zhang's multiscale flow equations [16] are used to respectively calculate the adsorbed layer flow and the intermediate continuum fluid flow.

The analysis is based on the following assumptions:

a. the two bearing surfaces are identical;
b. no interfacial slippage occurs on any interface;
c. the lubricating film is equivalently treated as isothermal by using the low value of the fluid viscosity in the condition of the frictional heating;
d. the condition is steady-state.

The total mass flow rate per unit contact length through the bearing is [16]:

$$q_m = -uh_{bf}\rho_{bf}^{eff} - \frac{uh}{2}\rho - \frac{h^3\rho}{12\eta}\frac{\partial p}{\partial x} + \frac{h_{bf}^3\rho_{bf}^{eff}}{\eta_{bf}^{eff}}\frac{\partial p}{\partial x}\left[\frac{F_1}{6} - \frac{\varepsilon}{1+\dfrac{\Delta x}{D}}\left(1+\frac{1}{2\lambda_{bf}} - \frac{q_o - q_o^n}{q_o^{n-1}-q_o^n}\frac{\Delta_{n-2}}{h_{bf}}\right)\right] +$$

$$+\frac{h^3\rho}{\eta_{bf}^{eff}}\frac{\partial p}{\partial x}\left[\frac{F_2\lambda_{bf}^2}{6} - \frac{\lambda_{bf}}{1+\dfrac{\Delta x}{D}}\left(\frac{1}{2}+\lambda_{bf} - \frac{q_o - q_o^n}{q_o^{n-1}-q_o^n}\frac{\Delta_{n-2}}{h}\right)\right], \tag{1}$$

where $\lambda_{bf} = h_{bf}/h$, h is the thickness of the continuum fluid film, n is the equivalent number of the fluid molecules across the adsorbed layer thickness, ρ is the fluid bulk density, η is the fluid bulk viscosity, D is the fluid molecule diameter, q_0 is the average value of Δ_{j+1}/Δ_j (Δ_j is the separation between the j^{th} and $(j+1)^{th}$ fluid molecules across the adsorbed layer thickness), Δx is the separation between the neighboring fluid molecules in the x coordinate direction (Fig. 1) in the adsorbed layer, Δ_{n-2} is the separation between the neighboring fluid molecules across the adsorbed layer thickness just on the boundary between the adsorbed layer and the continuum fluid film, ρ_{bf}^{eff} and η_{bf}^{eff} are respectively the average density and the effective viscosity of the adsorbed layer, $\rho_{bf}^{eff} = C_q\rho$,

$\eta_{bf}^{eff} = C_y\eta$; $F_1 = \eta_{bf}^{eff}\left(12D^2\psi + 6D\Phi\right)\Big/h_{bf}^3$,

$F_2 = 6\eta_{bf}^{eff}D(n-1)\left(l\Delta_{l-1}/\eta_{line,l-1}\right)_{avr,n-1}\Big/h_{bf}^2$,

$\varepsilon = \left(2DI + II\right)\Big/\left[h_{bf}(n-1)\left(\Delta_l/\eta_{line,l}\right)_{avr,n-1}\right]$,

$I = \sum_{i=1}^{n-1} i\left(\Delta_l/\eta_{line,l}\right)_{avr,i}$,

$II = \sum_{i=0}^{n-2}\left[i\left(\Delta_l/\eta_{line,l}\right)_{avr,i} + (i+1)\left(\Delta_l/\eta_{line,l}\right)_{avr,i+1}\right]\Delta_i$,

$\psi = \sum_{i=1}^{n-1} i\left(l\Delta_{i-1}/\eta_{line,j-1}\right)_{avr,i}$,

$\Phi = \sum_{i=0}^{n-2}\left[i\left(l\Delta_{l-1}/\eta_{line,l-1}\right)_{avr,i} + (i+1)\left(l\Delta_{l-1}/\eta_{line,l-1}\right)_{avr,i+1}\right]\Delta_i$,

$i\left(\Delta_l/\eta_{line,l}\right)_{avr,i} = \sum_{j=1}^{i}\Delta_{j-1}/\eta_{line,j-1}$,

$i\left(l\Delta_{l-1}/\eta_{line,l-1}\right)_{avr,i} = \sum_{j=1}^{i} j\Delta_{j-1}/\eta_{line,j-1}$; $\eta_{line,j-1}$ is the local viscosity between the j^{th} and $(j-1)^{th}$ fluid molecules across the adsorbed layer thickness, $\eta_{line,j}/\eta_{line,j+1} = q_0^{\gamma}$ and γ is constant.

Eq. (1) interprets that the total flow through the bearing consists of both the flow of the physically adsorbed molecule layer on the bearing surface and the flow of the continuum fluid film between the two adsorbed layers. It is particularly important when the bearing clearance becomes very low because of the thermoelastic deformation of the bearing surfaces.

The pressure gradient is obtained from Eq. (1) to be:

$$\frac{dp}{dx} = \frac{\frac{1}{2}u\rho h + q_m + uh_{bf}\rho_{bf}^{eff}}{\dfrac{c\rho h^3}{\eta} + \dfrac{d\rho_{bf}^{eff}h_{bf}^3}{\eta_{bf}^{eff}}}, \tag{2}$$

where

$$c = \frac{1}{C_y}\left[\frac{F_2\lambda_{bf}^2}{6} - \frac{\lambda_{bf}}{1+\dfrac{\Delta x}{D}}\left(\frac{1}{2}+\lambda_{bf} - \frac{q_0 - q_0^n}{q_0^{n-1}-q_0^n}\frac{\Delta_{n-2}\lambda_{bf}}{h_{bf}}\right)\right] - \frac{1}{12}, \tag{3}$$

$$d = \frac{F_1}{6} - \frac{\varepsilon}{1+\dfrac{\Delta x}{D}}\left(1+\frac{1}{2\lambda_{bf}} - \frac{q_0 - q_0^n}{q_0^{n-1}-q_0^n}\frac{\Delta_{n-2}}{h_{bf}}\right). \tag{4}$$

The thickness of the adsorbed layer is calculated as:

$$h_{bf} = nD + \Delta_{n-2}\frac{q_0 - q_0^n}{q_0^{n-1}-q_0^n}. \tag{5}$$

Eq. (5) can be derived according to the used adsorbed layer model shown by Zhang [16].

By incorporating the surface elastic deformation caused by the film pressure and the surface thermal distor-

tion, the continuum fluid film thickness is formulated as [2]:

$$h(x)=h_{oo}+f(x)-\frac{2}{\pi E_v}\int_0^{l_1+l_2}p(s)ln(x-s)^2ds+ +\frac{x^2}{2R_t}-2h_{bf}, \tag{6}$$

where h_{oo} is constant, p is the film pressure, E_v is the equivalent Young's modulus of elasticity of the two bearing surfaces, the second term is the function for the bearing geometrical shape and it is:

$$f(x)=\begin{cases}0 & 0<x\le l_1\\ \Delta h & l_1<x\le l_1+l_2\end{cases}, \tag{7}$$

the third term is for the total elastic deformation of the two bearing surfaces, the fourth term is for the total thermal distortions of the two bearing surfaces, and R_t is the compound thermal radius and calculated by [15]:

$$R_t=R_{t,a}R_{t,b}/\left(R_{t,a}+R_{t,b}\right). \tag{8}$$

Here, $R_{t,a}$ and $R_{t,b}$ are respectively the curvature radii of the upper and lower bearing surfaces induced by the surface thermal distortion and formulated as [15]:

$$R_{t,a}=k_a\rho_a c_a/\left(u\lambda_a\tau_{av}\alpha_a(1+\nu_a)(1-\chi)\right), \tag{9}$$

$$R_{t,b}=k_b\rho_b c_b/\left(u\lambda_b\tau_{av}\alpha_b(1+\nu_b)(1-\chi)\right), \tag{10}$$

where k, c, ρ, υ, α, λ and χ are respectively the thermal diffusivity, specific heat, density, Poisson's ratio, linear thermal expansion coefficient, frictional heat input rate of the contact surface and the rate of the frictional heating taken by the flow, the subscripts "a" and "b" respectively refer to the upper and lower bearing surfaces, and τ_{av} is the average value of the shear stresses respectively on the two bearing surfaces and calculated as:

$$\tau_{av}=\frac{f_a+f_b}{2}\frac{w}{l_1+l_2}, \tag{11}$$

where w is the load per unit contact length carried by the bearing, and f_a and f_b are respectively the friction coefficients on the upper and lower bearing surfaces.

By accounting for the non-continuum effect of the two physically adsorbed molecule layers and the Newtonian rheological behavior of the intermediate continuum fluid film, the shear stresses on the upper and lower bearing surfaces are respectively formulated as [16]:

$$\tau_a=-\frac{v_A-\bar{u}_a-\frac{dp}{dx}D\sum_{j=1}^{n-1}\frac{j\Delta_{j-1}}{\eta_{line,j-1}}}{\sum_{j=1}^{n-1}\frac{\Delta_{j-1}}{\eta_{line,j-1}}}-\frac{dp}{dx}D, \tag{12}$$

$$\tau_b=\frac{v_B-\bar{u}_b-\frac{\partial p}{\partial x}D\sum_{j=1}^{n-1}\frac{j\Delta_{j-1}}{\eta_{line,j-1}}}{\sum_{j=1}^{n-1}\frac{\Delta_{j-1}}{\eta_{line,j-1}}}+\frac{\partial p}{\partial x}D, \tag{13}$$

where v_A and v_B are respectively the velocities on the upper and lower boundaries of the continuum fluid film, and $\bar{u}_a$ and $\bar{u}_b$ are respectively the velocities of the fluid molecules on the upper and lower surfaces. Because of no interfacial slippage, it is obtained that $\bar{u}_a=0$ and $\bar{u}_b=-u$. v_A and v_B are respectively formulated as [16]:

$$v_B=\bar{u}_b+\frac{\partial p}{\partial x}D\sum_{j=1}^{n-1}\frac{j\Delta_{j-1}}{\eta_{\text{line},j-1}}+\frac{(\bar{u}_a-\bar{u}_b)\eta}{2\eta\sum_{j=1}^{n-1}\frac{\Delta_{j-1}}{\eta_{\text{line},j-1}}+h}\sum_{j=1}^{n-1}\frac{\Delta_{j-1}}{\eta_{\text{line},j-1}}-\frac{\partial p}{\partial x}\left(\frac{h}{2}+Dn\right)\sum_{j=1}^{n-1}\frac{\Delta_{j-1}}{\eta_{\text{line},j-1}}, \tag{14}$$

$$v_A=\bar{u}_b+\frac{\partial p}{\partial x}D\sum_{j=1}^{n-1}\frac{j\Delta_{j-1}}{\eta_{line,j-1}}+\frac{\bar{u}_a-\bar{u}_b}{\frac{2\eta}{h}\sum_{j=1}^{n-1}\frac{\Delta_{j-1}}{\eta_{line,j-1}}+1}\left(\frac{\eta}{h}\sum_{j=1}^{n-1}\frac{\Delta_{j-1}}{\eta_{line,j-1}}+1\right)-\frac{\partial p}{\partial x}\left(\frac{h}{2}+Dn\right)\sum_{j=1}^{n-1}\frac{\Delta_{j-1}}{\eta_{line,j-1}}. \tag{15}$$

According to the used adsorbed layer model [16], it is expressed that:

$$\sum_{j=1}^{i}\Delta_{j-1}/\eta_{\text{line},j-1}=\frac{\Delta_{n-2}[q_0^{(1+\gamma)(i-n+2)}-q_0^{-(n-2)(1+\gamma)}]}{\eta_{line,n-2}[q_0^{(1+\gamma)}-1]},\ \text{for } i=1,\ 2,\ \ldots,\ (n\text{-}1), \tag{16}$$

$$\sum_{j=1}^{i}j\Delta_{j-1}/\eta_{\text{line},j-1}=\frac{\Delta_{n-2}}{\eta_{line,n-2}}\left[\frac{q_0^{(2-n)(1+\gamma)}-q_0^{(1+\gamma)(i-n+2)}}{(q_0^{1+\gamma}-1)^2}+\frac{iq_0^{(1+\gamma)(i-n+2)}}{q_0^{1+\gamma}-1}\right],\ \text{for } i=1,\ 2,\ \ldots,\ (n\text{-}1). \tag{17}$$

Substituting Eq. (14) into Eq. (13) and also Eq. (15) into Eq. (12) gives the shear stresses on the upper and lower bearing surfaces on the j^{th} discretized point (Fig. 1) respectively as follows:

$$\tau_{a,j}=\eta\frac{\bar{u}_a-\bar{u}_b}{\dfrac{2\Delta_{n-2}\left[q_0^{(1+\gamma)}-q_0^{-(n-2)(1+\gamma)}\right]}{q_0^{(1+\gamma)}-1}+h_j}+\left.\frac{dp}{dx}\right|_j\left(\frac{h_j}{2}+Dn-D\right), \tag{18}$$

$$\tau_{b,j}=\eta\frac{\bar{u}_a-\bar{u}_b}{\dfrac{2\Delta_{n-2}\left[q_0^{(1+\gamma)}-q_0^{-(n-2)(1+\gamma)}\right]}{q_0^{(1+\gamma)}-1}+h_j}-\left.\frac{dp}{dx}\right|_j\left(\frac{h_j}{2}+Dn-D\right), \tag{19}$$

where by forward difference it is written that:

$$\left.\frac{dp}{dx}\right|_j=\frac{p_j-p_{j-1}}{\delta_x},\quad \text{for } j=1,2,\ldots,N, \tag{20}$$

here δ_x is the distance between the neighboring discretized points.

According to Eqs. (2) and (20), the film pressure on the j^{th} discretized point is:

$$p_j=p_0+\delta_x\sum_{i=1}^{j}\frac{\frac{1}{2}u\rho h_i+q_m+uh_{bf}\rho_{bf}^{eff}}{\frac{c\rho h_i^3}{\eta}+\frac{d\rho_{bf}^{eff}h_{bf}^3}{\eta_{bf}^{eff}}},\quad \text{for } j=1,2,\ldots,N. \tag{21}$$

The boundary condition gives that $p_0 = 0$.

The load per unit contact length carried by the bearing is:

$$w=\int_0^{l_1+l_2}p\,dx=\delta_x\sum_{j=1}^{N}p_j\ . \tag{22}$$

The frictional forces per unit contact length respectively on the upper and lower bearing surfaces are:

$$F_a=\int_0^{l_1+l_2}\tau_{a,j}\,dx=\delta_x\sum_{j=1}^{N}\tau_{a,j}\ , \tag{23}$$

$$F_b=\int_0^{l_1+l_2}\tau_{b,j}\,dx=\delta_x\sum_{j=1}^{N}\tau_{b,j}\ . \tag{24}$$

Then the friction coefficients on the two bearing surfaces are respectively:

$$f_a=\frac{|F_a|}{w}, \tag{25}$$

$$f_b=\frac{|F_b|}{w}. \tag{26}$$

3.2. Numerical calculation

In Eq. (6), there is the following integration term:

$$T=-\frac{2}{\pi E_v}\int_0^{l_1+l_2}p(s)\ln(x-s)^2ds\ . \tag{27}$$

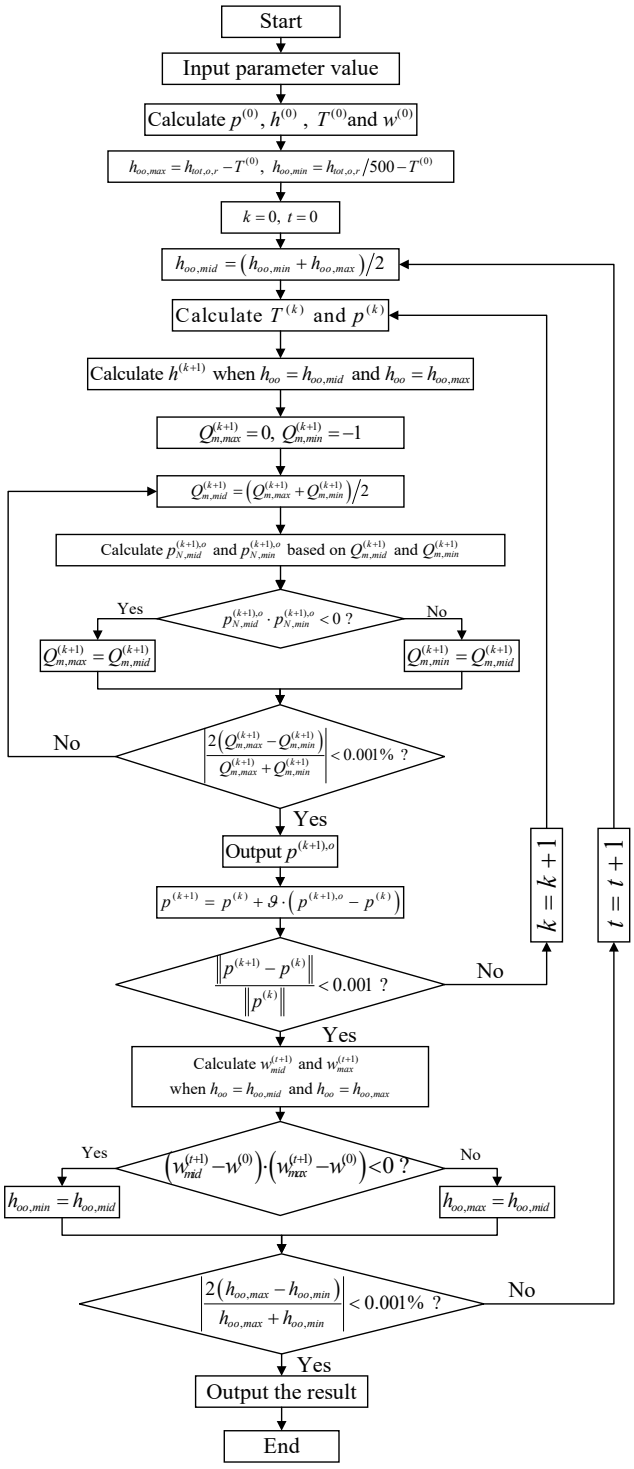

Fig. 2 The numerical solution procedure

Here, Eq. (27) is numerically calculated. Because of the surface elastic deformation under the film pressures and

the surface thermal distortion, the present problem is highly non-linear and the solution can only be numerically found. Fig. 2 shows the flow chart of the numerical calculation in the present study. $p^{(0)}$, $h^{(0)}$ and $w^{(0)}$ are respectively the film pressure distribution, the continuum fluid film thickness distribution and the carried load of bearing for the assumed rigid bearing surfaces; $T^{(0)}$ is the value of T under $p^{(0)}$. $h_{tot,o,r}$ is the surface separation on the exit of the bearing for rigid surfaces. k is the order number of the numerical iteration. $T^{(k)}$, $h^{(k)}$ and $p^{(k)}$ are respectively the value of T, h and p in the k^{th} iteration. $p_{N,mid}^{(k+1),o}$ and $p_{N,min}^{(k+1),o}$ are respectively the film pressures on the entrance of the bearing based on $Q_{m,mid}^{(k+1)}$ and $Q_{m,min}^{(k+1)}$. $Q_m^{(k+1)}$ is the dimensionless mass flow rate per unit contact length through the bearing obtained in the $(k+1)^{th}$ iteration by defining $Q_m = q_m/(u\rho h_{tot,o,r})$; ϑ is the relaxation factor. $w_{mid}^{(t+1)}$ and $w_{max}^{(t+1)}$ are respectively the values of the bearing load based on $h_{oo} = h_{oo,mid}$ and $h_{oo} = h_{oo,max}$.

4. Input Parameter Values for Calculation

It is assumed that $\eta_{line,j}/\eta_{line,j+1} = q_0^{\gamma}$ [16]. The equation formulations for C_q and C_y were shown in [15]. The regressed equation formulations for F_1, F_2 and ε were shown in [16]. The weak, medium and strong fluid-surface interactions were respectively considered. The corresponding parameter values respectively for characterizing these three interactions were shown in [15].

The two bearing surfaces are made of steel. The input values of the other parameters for calculation are as follows:

$N = 2000$, $D = 0.5$ nm, $\Delta x / D = \Delta_{n\text{-}2} / D = 0.15$,
$E_v = 209$ GPa, $\eta = 0.005$ Pa·s, $l_1 = l_2 = 0.2$ m, $\Delta h = 20$ μm,
$\vartheta = 0.0001$, $\lambda_a = \lambda_b = 0.5$, $k_a = k_b = 1.53\times10^{-5}$ m^2/s,
$c_a = c_b = 400$ J/(kg·°C), $\alpha_a = \alpha_b = 1.3\times10^{-5}$, $v_a = v_b$ 0.3,
$\chi = 0$, $\rho_a = \rho_b = 7800$ kg/m^3.

5. Results

5.1. Minimum surface separation

Fig. 3, a shows that when the surface thermal distortion is neglected, for a given load the value of the minimum surface separation is rapidly increased with the increase of the sliding speed. However, Fig. 3, b shows that when the surface thermal distortion is incorporated, there is the optimum value of the sliding speed which gives the greatest value of the minimum surface separation; The sliding speed deviating from this optimum one results in the reduction of the minimum surface separation. The high sliding speed causes the severe frictional heating and the significant surface thermal distortion and consequently pronouncedly modifies the surface separation profile and reduces the minimum surface separation. In the condition of heavy loads and high sliding speeds (e.g. $w = 5000$ kN/m and $u \geq 15$ m/s), owing to the surface thermal distortion, the minimum surface separation is less than 0.8 μm and more than 20 times smaller than the classical calculation as shown in Fig. 3, a; For $u = 105$ m/s, such a difference reaches 100 times. These results support the arguments on the experimental findings of the hydrodynamic film breakdown in large thrust bearings which ascribed the film breakdown to the pad thermal distortion [8-10].

Fig. 4 shows that in the condition of heavy loads and high sliding speeds ($u = 20$ m/s), when the surface elastic deformation is considered but the surface thermal distortion is neglected, the calculated minimum surface separations are a bit lower than the classical hydrodynamic theory calculation, which is based on the assumption of rigid surfaces. However, when the effect of the surface thermal distortion is further incorporated, the calculated minimum surface separations are 1 to 2 orders smaller than the classical calculations and they are much more rapidly reduced with the increase of the load than the classical hydrodynamic theory description. These indicate the severe worsening condition of the thrust bearing under heavy loads owing to the surface thermal distortion and follow the experimental observations [8-10].

Fig. 5, a shows that when the minimum surface separation $h_{tot,min}$ is reduced to below 0.3 μm owing to the

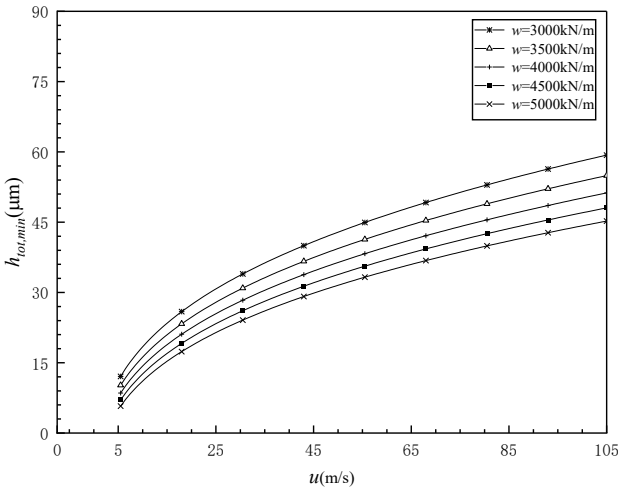

a

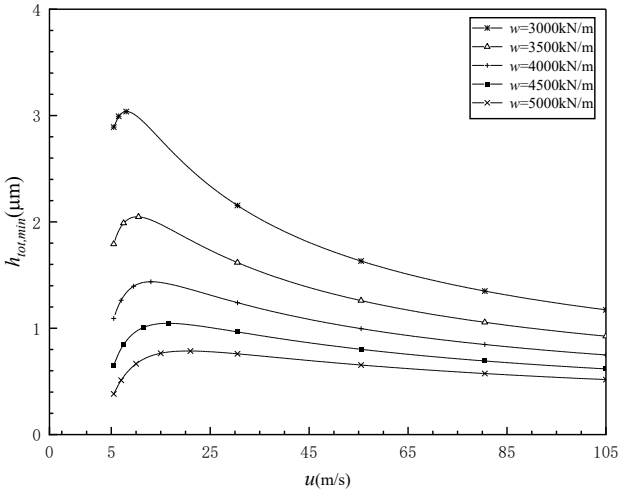

b

Fig. 3 Variations of the minimum surface separation with the sliding speed for different loads for the strong fluid-surface interaction: a – for elastic surfaces without thermal distortion, b – for elastic surfaces with thermal distortion

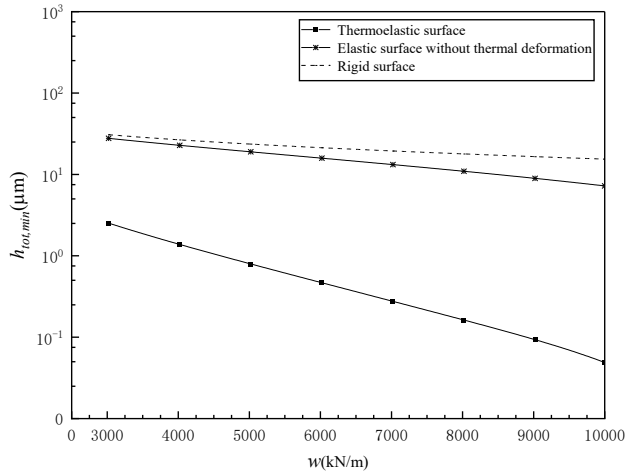

Fig. 4 Variation of the minimum surface separation with the load for different contact regimes when u = 20 m/s and the fluid-surface interaction is strong

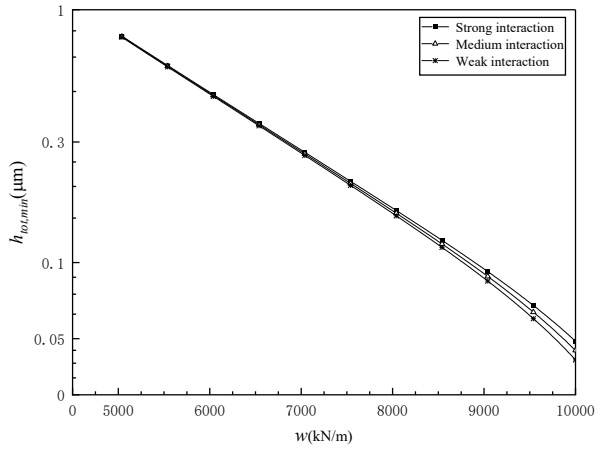

a

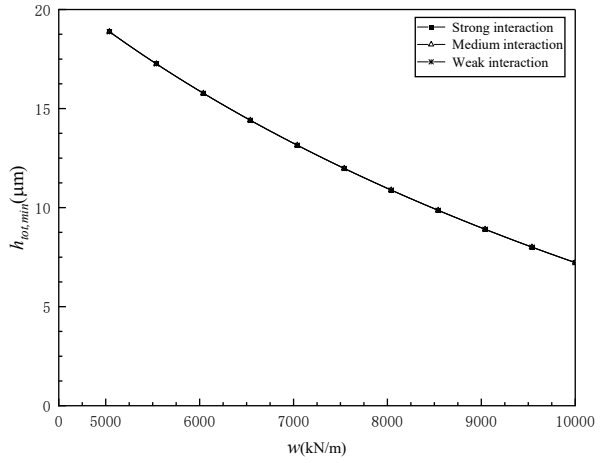

b

Fig. 5 Variations of the minimum surface separation with the load for different fluid-surface interactions when u = 20 m/s: a – for elastic surfaces with thermal distortion, b – for elastic surfaces without thermal distortion

effect of the surface thermal distortion or the load is greater than 7000 kN/m, the effect of the fluid-surface interaction is noticeable due to the effect of the physically adsorbed layer. When $h_{tot,min}$ is as low as only several tens nanometers for the load greater than 8500 kN/m, the strong fluid-surface interaction gives the much higher minimum surface separations than the weak and medium fluid-surface interactions. However, Fig. 5, b shows that the effect of the fluid-surface interaction on the minimum surface separation is negligible for the same operating conditions if the surface thermal distortion is ignored; It is due to the resulting minimum surface separations (more than 7.5 μm) far greater than the thickness of the physically adsorbed layer so that the effect of the adsorbed layer is negligible. The comparisons between Figs. 5, a-b show that in studying the performance of the hydrodynamic big-size thrust bearing in the condition of heavy loads and high sliding speeds, the combined effects of the surface thermal distortion and the physically adsorbed layer on the bearing surface should be considered. This demands the multiscale lubrication analysis by incorporating both the adsorbed layer flow and the intermediate continuum fluid flow.

5.2. Film pressure distribution and surface separation profile

Fig. 6 shows that owing to the effect of the surface thermal distortion, the maximum film pressure moves

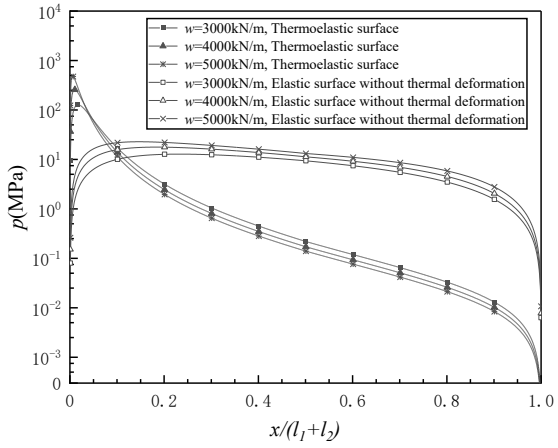

Fig. 6 Film pressure distributions in the bearing for different contact regimes for the strong fluid-surface interaction when u = 20 m/s

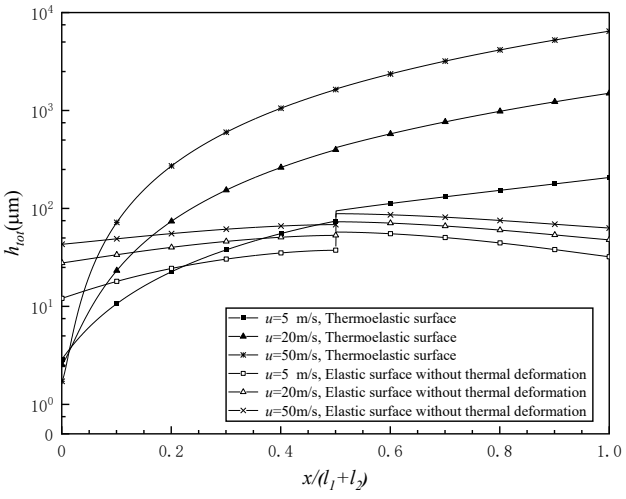

Fig. 7 Surface separation profiles for different contact regimes when w = 3000 kN/m and the fluid-surface interaction is strong

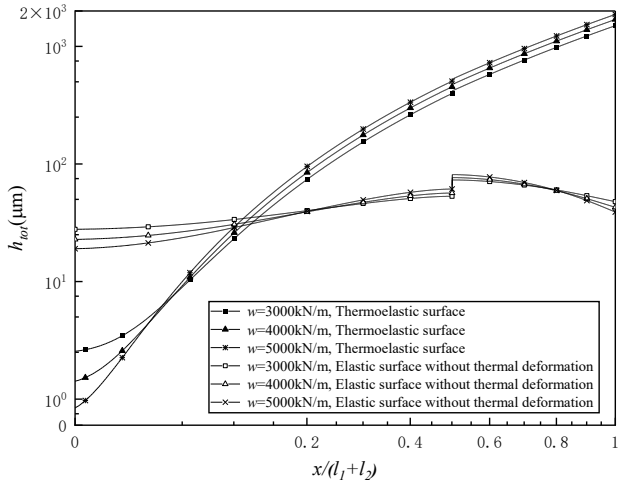

Fig. 8 Surface separation profiles for different contact regimes when u = 20 m/s and the fluid-surface interaction is strong

closer to the exit of the bearing and the magnitudes of the pressure gradients in the outlet zone of the bearing and particularly around the location where the maximum film pressure occurs are much greater than those by neglecting the surface thermal distortion.

Figs. 7-8 show that in the condition of heavy loads and high sliding speeds, the severe surface thermal distortion largely modifies the surface separation profiles and the step of the bearing is not visible.

5.3. Friction coefficient

Figs. 9, a-b show that owing to the surface thermal distortion, the friction coefficient on the upper i.e. stationary bearing surface is much smaller than those classically calculated, while the friction coefficient on the lower i.e. moving bearing surface is significantly greater than the latter. This obvious discrepancy is due to the large magnitudes of the pressure gradients occurring in the bearing due to the surface thermal distortion.

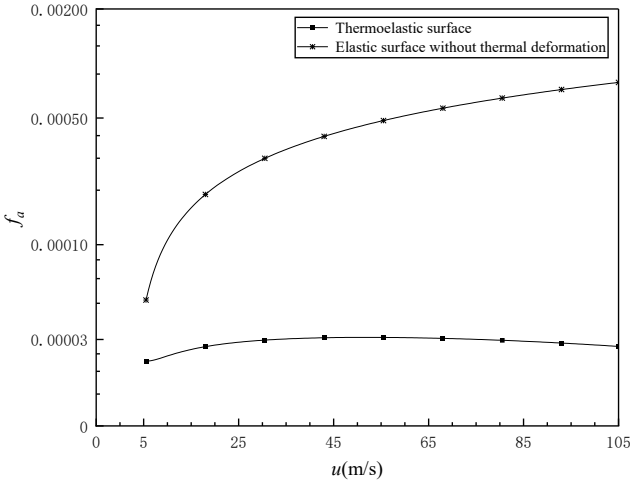

a

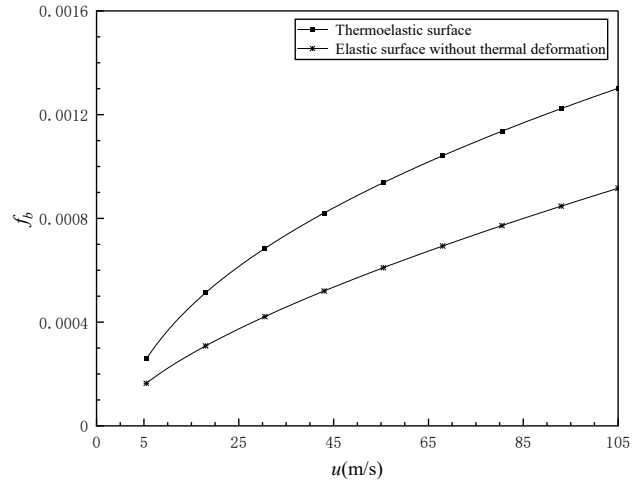

b

Fig. 9 Friction coefficients in the bearing for different contact regimes when w = 3000 kN/m and the fluid-surface interaction is strong: a – on the upper bearing surface, b – on the lower bearing surface

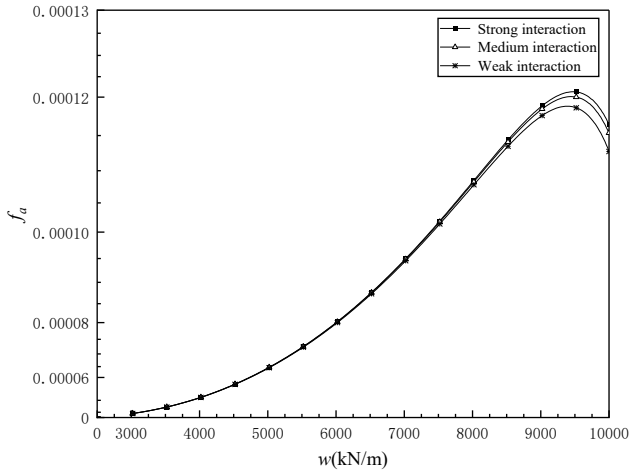

a

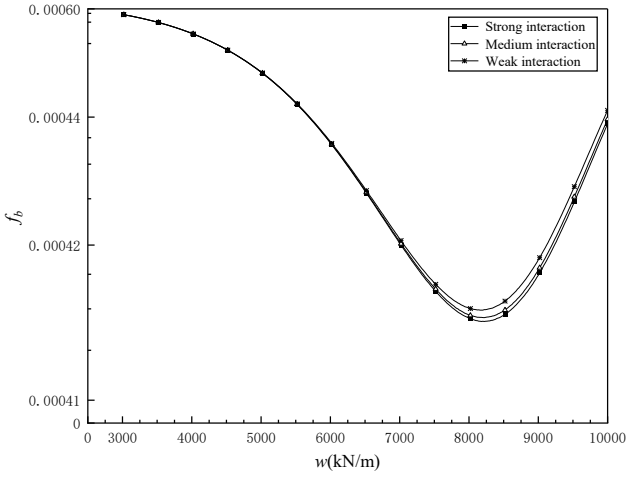

b

Fig. 10 Friction coefficients in the bearing for different fluid-surface interactions when u = 20 m/s and the effect of the surface thermal distortion is incorporated: a – on the upper bearing surface, b – on the lower bearing surface

Figs. 10, a-b show the influence of the fluid-surface interaction on the friction coefficient of the bearing when u = 20 m/s and the effect of the surface thermal distortion is incorporated. When the load is greater than 7000 kN/m, the effect of the fluid-surface interaction on the friction coefficient of the bearing is appreciable, it a

little increases the friction coefficient on the upper bearing surface but a little reduces the friction coefficient on the lower bearing surface if the fluid-surface interaction is strong. Such phenomena occur in the condition of low surface separations. While for relatively high surface separations i.e. for the loads smaller than 7000 kN/m, they are absent and indicate the negligible effect of the fluid-surface interaction.

6. Conclusions

The combined effects of the surface thermoelastic deformation and the physically adsorbed layer on the surface are numerically investigated in the hydrodynamic big-size step bearing in the condition of heavy loads and high sliding speeds by using the multiscale lubrication analysis. The studied bearing mimics those used in hydrogenerators or hydro turbines. Exemplary calculations were made and the conclusions are drawn as follows:

a. The effect of the surface thermal distortion is very significant and it can reduce the minimum surface separation by 1 to 2 orders in the bearing; While the effect of the physically adsorbed layer significantly plays when the minimum surface separation is below 0.3 μm and it can significantly increase the minimum surface separation for the strong fluid-bearing surface interaction.
b. The surface thermal distortion largely modifies the surface separation profile and the bearing original geometry of the step is even not visible. It much increases the magnitudes of the pressure gradients around the location where the maximum film pressure occurs.
c. For sufficiently heavy loads, the effect of the physically adsorbed layer on the friction coefficient of the bearing is appreciable because of the low surface separations.
d. In studying the performance of the hydrodynamic big-size thrust bearing, the combined effects of the surface thermal distortion and the physically adsorbed layer on the bearing surface should be considered.
e. In the subsequent research, the mixed lubrication model should be developed for the studied bearing by incorporating the effect of the surface roughness. It may be important when the bearing clearance is low.

References

1. **Yuan, J. H.; Medley, J. B.; Ferguson, J. H.** 1999. Spring-Supported Thrust Bearings Used in Hydroelectric Generators: Laboratory Test Facility, Tribology Transactions 42(1): 126-135. http://doi.org/10.1080/10402009908982199.
2. **Ettles, C. M.** 1980. Size effects in tilting pad thrust bearings, Wear 59(1): 231-245. https://doi.org/10.1016/0043-1648(80)90281-1.
3. **Pinkus, O.; Sternlicht, B.** 1961. Theory of Hydrodynamic Lubrication. New York: McGraw-Hill. 465p.
4. **Zhai, L. M.; Luo, Y. Y.; Wang, Z. W.; Liu, X.; Xiao, Y. X.** 2017. A review on the large tilting pad thrust bearings in the hydropower units, Renewable and Sustainable Energy Reviews 69: 1182-1198. https://doi.org/10.1016/j.rser.2016.09.140.
5. **Peterson, J.; Finn, W. E.; Dareing, D. W.** 1994. Non-Newtonian Temperature and Pressure Effects of a Lubricant Slurry in a Rotating Hydrostatic Step Bearing, Tribology Transactions 37(4): 857-863. https://doi.org/10.1080/10402009408983369.
6. **Andharia, P. I.; Pandya, H. M.** 2018. Effect of Longitudinal Surface Roughness on the Performance of Rayleigh Step Bearing, International Journal of Applied Engineering Research 13(21): 14935-14941.
7. **Vakilian, M.; Nassab, S. A. G.; Kheirandish, Z.** 2013. Study of inertia effect on thermohydrodynamic characteristics of Rayleigh step bearings by CFD method, Mechanics & Industry 14(4): 275-285. https://doi.org/10.1051/meca/2013065.
8. **Chambers, W. S.; Mikula, A. M.** 1988. Operational Data for a Large Vertical Thrust Bearing in a Pumped Storage Application, Tribology Transactions 31(1): 61-65. https://doi.org/10.1080/10402008808981798.
9. **Ettles, C. M.; Seyler, J.; Bottenschein, M.** 2003. Some Effects of Start-Up and Shut-Down on Thrust Bearing Assemblies in Hydro-Generators, ASME Journal of Tribology 125(4): 824-832. https://doi.org/10.1115/1.1576428.
10. **Kawaike, K.; Okano, K.; Furukawa, Y.** 1979. Performance of a Large Thrust Bearing with Minimized Thermal Distortion, ASLE Transactions 22(2): 125-134. https://doi.org/10.1080/05698197908982908.
11. **Wodtke, M; Schubert, A; Fillon, M; Wasilczuk, M; Pajączkowski, P.** 2014. Large hydrodynamic thrust bearing: Comparison of the calculations and measurements, Proceedings of the Institution of Mechanical Engineers, Part J: Journal of Engineering Tribology 228(9): 974-983. https://doi.org/10.1177/1350650114528317.
12. **Kim, K. W.; Tanaka, M.; Hori, Y.** 1983. A Three-Dimensional Analysis of Thermohydrodynamic Performance of Sector-Shaped, Tilting-Pad Thrust Bearings, ASME Journal of Lubrication Technology 105(3): 406-412. https://doi.org/10.1115/1.3254625.
13. **Ettles, C. M.; Anderson, H. G.** 1991. Three-Dimensional Thermoelastic Solutions of Thrust Bearings Using Code Marmac1, ASME Journal of Tribology 113: 405-412. https://doi.org/10.1115/1.2920636.
14. **Brockett, T. S.; Barrett, L. E.; Allaire, P. E.** 1996. Thermoelastohydrodynamic analysis of fixed geometry thrust bearings including runner deformation, Tribology Transactions 39(3): 555-562. http://doi.org/10.1080/10402009608983566.
15. **Zhang, Y. B.** 2014. Lubrication Analysis for a Line Contact Covering from Boundary Lubrication to Hydrodynamic Lubrication: Part I-Micro Contact Results, Journal of Computational and Theoretical Nanoscience 11(1): 62-70. https://doi.org/10.1166/jctn.2014.3318.
16. **Zhang, Y. B.** 2020. Modeling of flow in a very small surface separation, Applied Mathematical Modelling 82: 573-586. https://doi.org/10.1016/j.apm.2020.01.069.

X. Ye, Y. Zhang

EFFECT OF SURFACE THERMOELASTIC DEFORMATION ON THE PERFORMANCE OF THE HYDRODYNAMIC BIG-SIZE STEP BEARING

S u m m a r y

The multiscale lubrication analysis is presented for estimating the performance of the hydrodynamic big-size step bearing by incorporating the effects of the surface thermoelastic deformation and the lubricant molecule layers physically adsorbed to the bearing surface. The numerical calculation results show that in the condition of heavy loads and high sliding speeds, the effect of the surface thermoelastic deformation can reduce the minimum surface separation by 1 to 2 orders, while the effect of the physically adsorbed layer on the bearing surface significantly increases the minimum surface separation especially for the strong fluid-bearing surface interaction; The effect of the surface thermoelastic deformation largely modifies both the film pressure profile and the surface separation profile in the bearing; It also obviously changes the friction coefficient of the bearing. The effect of the physically adsorbed layer significantly influences the friction coefficient of the bearing only in the condition of heavy loads and high sliding speeds, which yields very low surface separations.

Keywords: adsorbed layer, film pressure, friction coefficient, hydrodynamic lubrication, surface thermoelastic deformation, thrust bearing.

Received March 3, 2025
Accepted June 25, 2025